The sky characterization according to the CIE Standard General Sky: comparative analysis of three classification methods

Ignacio García[a,b,*] Marian de Blas[a,b] and José Luis Torres[a,b]

[a] Department of Engineering, Public University of Navarre, Campus Arrosadía, 31006 Pamplona, Spain.

[b] Institute of Smart Cities (ISC), Public University of Navarre, Campus Arrosadía, 31006 Pamplona, Spain.

* Corresponding author: Tel.: +34 948 168405, Fax: +34 948 169148, email: ignacio.garcia@unavarra.es

ABSTRACT

Since the publication of the standard sky luminance distributions (SSLD) that was consolidated in the ISO 15469:2004(E)/CIE S 011/E:2003, numerous procedures have emerged for the characterization of the sky condition according to that standard. Precisely, the use of different procedures for the classification of the skies of a certain place according to the ISO/CIE standard can lead to obtain different frequencies of sky types. The existing uncertainties in the characterization of the sky condition according to the CIE Standard General Sky as a consequence of the classification procedure used are analyzed in this study. For this, three different classification procedures are used to characterize the sky radiance and luminance distribution measurements made by means of a sky-scanner in Pamplona (Spain) from 2007 to 2013. That is, (1) a method focused on determining the relative gradation and indicatrix functions, (2) a method based on the comparison of measured and standard luminances normalized against the horizontal diffuse illuminance, and (3) a new high-spatial-resolution approach that compares measured and standard luminances relative to zenith. In general terms, it is concluded that there is some uncertainty in the classification depending on the procedure used to characterize the sky.

KEYWORDS

Sky luminance distribution; Classification procedures; CIE Standard Sky

NOMENCLATURE

b_p	bands in which the sky patches are distributed.
D_v	horizontal diffuse illuminance.
D_{vp}	horizontal diffuse illuminance coming from sky patch p.
f	indicatrix function.
g	gradation function.
E_v	horizontal extraterrestrial illuminance.
$\overline{E_v}$	average horizontal extraterrestrial illuminance.
F_c	correction factor.
F_g	geometric factor.
F_{gp}	geometric factor of sky patch p.
G_v	global horizontal illuminance.
$\overline{G_v}$	average global horizontal illuminance.
$L(Z,\gamma)$	luminance of any sky point with coordinates (Z,γ).
$l(Z,\gamma)$	luminance relative to zenith of any sky point with coordinates (Z,γ).
L_p	measured luminance of a sky patch.
l_p	measured luminance relative to zenith of a sky patch.
$L_{p,st}$	luminance of a sky patch corresponding to a standard sky.
$l_{p,st}$	luminance relative to zenith of a sky patch corresponding to a standard sky.
L_{pn}	normalized measured luminance of a sky patch.
$L_{pn,st}$	normalized luminance of a sky patch corresponding to a standard sky.
L_Z	zenith luminance.
n_a	number of points considered in each almucantar.
n_p	total number of sky patches.
n_{pb}	number of patches in each band.
p	sky patch.
R	distance between a pixel and the center of the image.
S_d	summation of the F_g corresponding to the patches considered in each scan.
Z	zenith angle of a sky point.
Z_S	zenith angle of the sun.
α	angle of elevation of a sky point above the horizon.
α_S	angle of elevation of the sun above the horizon.
γ	azimuth angle of a sky point measured from the south.
γ_S	azimuth angle of the sun measured from the south.
χ	angle between the sun and a sky point.

ABBREVIATION

CIE	International Commission on Illumination.
FOV	field of view.
IDMP	International Daylight Measurement Program.
IDW	inverse distance weighting.
NL	method of normalized luminances.
RGI	method of relative gradation and indicatrix.
RMSD	root-mean-square deviation.
RZL	method of relative zenith luminances.
SSLD	standard sky luminance distributions.

1. INTRODUCTION

Overcast or clear skies have characteristics that can easily be modeled, which means that the first models of angular distribution of radiance and luminance in the sky vault were dedicated to a single sky type. This is the case of the Moon and Spencer (1942) model for overcast skies and the Kittler (1965) model for clear skies that resulted in two standards adopted by the International Commission on Illumination (CIE) (CIE, 1955, 1973, respectively). In addition, the fact that they are of interest for certain purposes has made them popular in engineering applications. However, clear and overcast skies represent only the extremes of a wide range of variability of the real skies. In order to deal with this reality, a second type of angular distribution models for all sky conditions emerged, including the models developed by Perraudeau (1988), Matsuura and Iwata (1990), Perez et al. (1990), Brunger and Hooper (1993), Perez et al. (1993), Igawa et al. (2004) and Igawa (2014). For their part, Kittler et al. (1998, 1997) proposed a set of 15 sky standards whose luminance distributions, called standard sky luminance distributions (SSLD), were described in the SSLD catalog. This proposal was consolidated in 2004 with the CIE Standard General Sky (ISO 15469:2004(E)/CIE S 011/E:2003, 2004) that incorporated the existing CIE standard skies.

Though the CIE Standard General Sky was published in 2004, several authors had proposed before 2004 different methodologies for the characterization of the sky according to the sky standards described by Kittler et al. (1997,1998). Some of these methodologies are described in the following subsections. In fact, the sky type characterization has been discussed since the publication of the SSLD catalog. In this sense, numerous procedures aimed at this purpose can be found in the scientific literature that, in a general way, can be grouped into three families of widely used methods:

- Lz/Dv ratio method.
- Normalized luminances method.
- Relative gradation and indicatrix method.

A literature review of the three families of methods is presented in the following sections. Though, regardless of the methods included in each of these three families, there are other methodologies as the one proposed by Markou et al. (2007). This method was used for the classification of sky luminance distributions provided by a sky-scanner in Garston (south England). The classification was carried out through a multivariate statistical procedure that chains a factor analysis and a cluster analysis. For the interpretation of the groupings between the individuals in the experimental sample, the underlying physical processes through the gradation and indicatrix functions were considered. The authors pointed out that, by applying this procedure, the sky classification observed in the three main categories of sky conditions (clear, overcast and intermediate skies) was quite similar to that achieved by the Lz/Dv ratio method.

1.1. Method of the Lz/Dv ratio

In the research of Kittler et al. (1997,1998), in which a set of standard skies was defined, the possibility of determining the standard sky types was offered by means of a family of 15 curves, one for each standard sky, parameterized according to the ratio of the the zenith luminance (Lz) to the horizontal diffuse illuminance (Dv). For this reason, this procedure is known by some authors as the SSLD method. When characterizing a certain sky, it is necessary to calculate the Lz/Dv ratio at that specific time and to identify the closest curve to the calculated value from the set of the 15 standard curves. This method was used by Bartzokas et al. (2003) for the characterization of the skies of Central Europe and the Mediterranean in winter, specifically in the cities of Bratislava (Slovakia) and Athens (Greece). It was also used by Markou et al. (2005) for the classification of skies over Sheffield (Central England) during winter and in Mukherjee (2014) for the classification of skies over Delhi (India) during winter and summer seasons from illuminance measurements made at Central Building Research Institute (Roorkee, India) under the International Daylight Measurement Program (IDMP) station and modeled zenith luminance. The method of the Lz/Dv ratio was also recommended by the CIE Standard General Sky Guide (CIE, 2014), which also included two proposals for the calculation of gradation and indicatrix functions from scanned data.

As numerous studies have pointed out, this method presents an important disadvantage since, from a solar elevation of 37º upwards, the Lz/Dv curves converge, thus making it difficult to discriminate the standard sky corresponding to the moment under analysis. In order to overcome this drawback, Bartzokas et al. (2005) proposed a modification of the SSLD method that allows to distinguish standard skies for higher solar elevations. The skies of Bratislava and Athens were again classified using the same database as in the work of Bartzokas et al. (2003). In cases of overlap between the Lz/Dv curves, an observation can be classified in more than one sky standards; then the ratio of global horizontal illuminance (Gv) to horizontal extraterrestrial illuminance (Ev) for the specific observation is further compared with the average ratios ($\overline{Gv}/\overline{Ev}$) estimated from all observations at the same solar altitude for a particular standard sky. The observation is then classified in that standard sky for which the value of Gv/Ev is the nearest to the $\overline{\mathrm{Gv}}/\overline{\mathrm{Ev}}$ value.

Li and Tang (2008) presented a classification of the Hong Kong skies from sky luminance measurements using three sky classification procedures: (1) the method proposed by Li et al. (2003), described in Subsection 1.2, (2) the modification of the SSLD method described by Bartzokas et al. (2005), and (3) a new variation of the SSLD method for low latitudes such as those that can be found in the location of the Li and Tang's study. In this last approach there was proposed the use of a hybrid daylight variable consisting of the pair Lz/Dv - Gv/Ev, already suggested by Kittler and Darula (2002), to discriminate among the three typical sky conditions (overcast, partly cloudy and clear). The use of the ratios Lz/Dv and Dv/Ev was proposed to distinguish between the five overcast ISO/CIE sky types. Regarding the types corresponding to partly cloudy conditions, the luminous turbidity proposed by Kittler et al. (1998) was used except for the sky standard type 6 that was discriminated by the absence of direct-beam solar illuminance. The same daylight variables were used to categorize the five clear standard skies.

1.2. Method of the normalized luminances

A procedure for sky classification according to the sky standards proposed by Kittler et al. (1997,1998) can be found in a study by Tregenza (1999). In this procedure, the luminances measured at a sky patch by a sky-scanner were normalized against Dv obtained from the integration of the luminances of all sky patches over the whole sky vault. Secondly, the luminances corresponding to the center of each patch were calculated and normalized against Dv for each of the 15 standard types. Finally, the root-mean-square deviation (RMSD) was computed between the measured and calculated luminances corresponding to each standard sky and the standard sky exhibiting the lowest RMSD was selected.

Tregenza (2004) proposed a variation to his previous method (Tregenza, 1999) that affects the calculated luminance assigned to each sky patch. Instead of assigning the value corresponding to the center of the patch, the average value of those calculated at its four vertices was assigned. As in the original procedure, the standard type is selected whose distribution is better adjusted to the normalized measured distribution by calculating the RMSD. The last method was used, among others, for determining standard skies for Hong Kong (Ng et al., 2007) and for the classification of skies in Pamplona (Spain) during the summer (Torres et al., 2010a) and winter (Torres et al., 2010b) periods. This method was also used by Torres et al. (2014) for the classification of skies in Pamplona and Arcavacata di Rende (Italy) with the aim of generating synthetic standard sky types series using Markov transition matrices.

In line with Tregenza (1999), Li et al. (2003) conducted a classification of the 15 sky luminance patterns in Hong Kong from luminance measurements. Again, the luminance distributions corresponding to the 15 standard types were compared with the measured luminance values. However, in this case the sky luminance distributions were normalized by the normalization ratio proposed by Littlefair (1994a, 1994b). This parameter, which is calculated for each standard sky type, results from the ratio of the integration of the measured absolute luminances to the integration of the modeled luminances corresponding to the standard. The sky type is selected considering the RMSD between the measured and modeled luminances. Suárez-García et al. (2018) used two methods of normalized luminances described for the characterization of the skies at Burgos (Spain): the Tregenza (2004) method and that of Li et al. (2003). Both procedures were compared observing a good agreement between them.

1.3. Method of the relative gradation and indicatrix

Wittkopf and Soon (2007) compared three procedures for the analysis of the luminance distribution in the sky vault of Singapore. The selected procedures were (1) the SSLD method, (2) the procedure of Tregenza (1999, 2004) and (3) a method based on the determination of the relative gradation and indicatrix functions from sky luminance measurements. Specifically, within the third method, the determination of the indicatrix function was based on the proposals by Kittler et al. (1992) and Kittler (1993). The procedure has a series of limitations when the solar elevation is below 45º, so a modification was proposed.

Kobav et al. (2012) characterized the skies of Lyon (France) from luminance angular distribution data measured at their IDMP station. As in the previous method, the classification procedure involved the determination of the gradation group and the relative indicatrix group, separately. The standard sky type was obtained by combining both functions. The combination of the six possible groups of gradation with the six possible groups of indicatrix results in 36 sky types. However, only 15 of them are considered standards by ISO/CIE. Therefore, a proposal was included (in the form of a table) for the assignment of non-standardized gradation and indicatrix group combinations to standard sky types.

According to this review, it can be appreciated that the use of different procedures for the sky classification in a certain location considering the ISO/CIE standard can lead to obtaining different frequencies of sky types. In the present paper, the existing uncertainties in the characterization of the sky condition according to the CIE Standard General Sky as a consequence of the applied classification procedure are analyzed. For this, the classifications obtained by applying three procedures with a different approach are compared. Although the definition of the ISO/CIE standard skies are based solely on photometric variables the possibility of classifying skies from radiance instead of luminance is also studied. To this end it has been analyzed to what extent the classification obtained considering the luminance fits to that obtained by radiance. Likewise, obtained differences in the sky type when classifying the two parts of the sky separated by the solar meridian are compared.

The structure of this paper is as follows: the CIE Standard General Sky is described in Section 2. The meteorological data used in this study, the measurement equipment used to obtain the data and the quality-control procedures applied are detailed in Section 3. Section 4 describes the three different procedures applied to determine the CIE Standard General Sky type. In Section 5, the results obtained after the sky classification are presented and analyzed. That is, the comparison between the ISO/CIE standard sky types obtained from luminance and radiance measurements (Section 5.1), the comparison between the sky types obtained by each of the three procedures described (Section 5.2) and the analysis of the sky classification symmetry (Section 5.3). A revised proposal for allocating the non-standardized combinations of indicatrix and gradation functions to the ISO/CIE standard types is analysed in Section 5.4. The conclusions obtained are detailed in Section 6.

2. CIE STANDARD GENERAL SKY

According to the ISO 15469:2004(E)/CIE S 011/E:2003 (2004), the luminance relative to zenith at a given point in the sky vault, $l(Z,\gamma)$, is given by the Equation (1).

$$l(Z,\gamma) = \frac{L(Z,\gamma)}{L_Z} = \frac{f(\chi)\cdot g(Z)}{f(Z_S)\cdot g(0)}, \quad (1)$$

where $L(Z,\gamma)$ is the luminance of any sky point given its zenith angle (Z) and azimuth (γ), f is the indicatrix function, g is the gradation function, Z_S is the solar zenith angle and χ is the angular distance between the sun and a sky vault point.

The indicatrix function, $f(\chi)$, in Equation (2) expresses the relationship between the luminance at a sky point with an angular distance from the sun (χ) and that at the point where χ is equal to 90º. The indicatrix function is related to the scattering of solar radiation as it passes through the atmosphere.

$$f(\chi) = 1 + c[\exp(d\chi) - \exp(d\pi/2)] - e\cos^2\chi. \tag{2}$$

The gradation function, $g(Z)$, which obeys to the Equation (3), characterizes the luminance variation from the zenith ($Z = 0$) to the horizon ($Z = 90º$).

$$g(Z) = 1 + a\exp(b/\cos Z). \tag{3}$$

The relative gradation function is obtained by means of the quotient of the gradation corresponding to a given zenith angle, $g(Z)$, to the one corresponding to zenith, $g(0)$, as described by Equation (4).

$$\frac{g(Z)}{g(0)} = \frac{1 + a\exp(b/\cos Z)}{1 + a\exp(b)}. \tag{4}$$

Coefficients (a, b, c, d, e) included in Equations (2) and (3) depend on the standard sky type (see Table I). The ISO/CIE standard defines six groups of coefficients (a, b) and six groups of coefficients (c, d, e) that correspond to the same number of gradation and indicatrix groups, represented in Figure 1. Consequently, in order to calculate the angular distribution of relative luminance in the sky vault at any given moment by applying Equation (1), it is necessary to know first the type of sky at that moment.

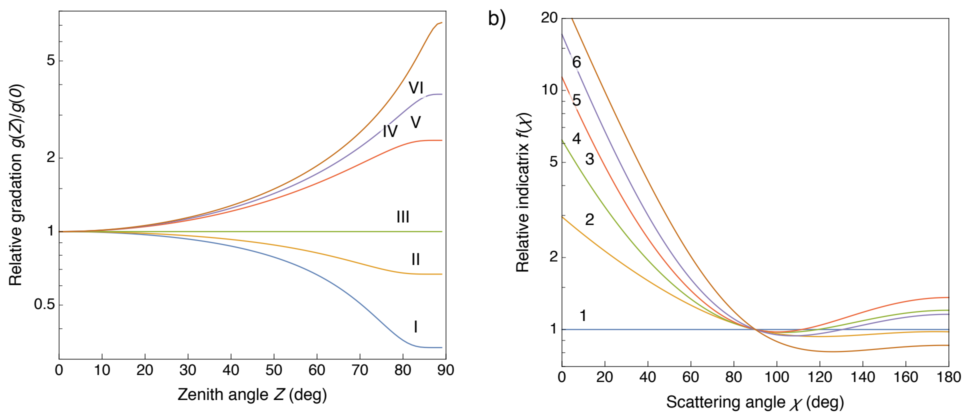

Figure 1. Standard gradation profiles (a) and standard indicatrix profiles (b).

Table I. CIE Standard General Sky parameters (ISO 15469:2004(E)/CIE S 011/E:2003, 2004).

Type	Gradation group	Indicatrix group	a	b	c	d	e	Description of luminance distribution
1	I	1	4.0	-0.7	0.0	-1.0	0.0	Overcast CIE Standard Overcast Sky, steep gradation and with azimuthal uniformity.
2	I	2	4.0	-0.7	2.0	-1.5	0.15	Overcast, with steep gradation and slight brightening towards the sun.
3	II	1	1.1	-0.8	0.0	-1.0	0.0	Overcast, moderately graded, with azimuthal uniformity.
4	II	2	1.1	-0.8	2.0	-1.5	0.15	Overcast, moderately graded, with slight brightening towards the sun.
5	III	1	0.0	-1.0	0.0	-1.0	0.0	Overcast, foggy or cloudy, with overall uniformity.
6	III	2	0.0	-1.0	2.0	-1.5	0.15	Partly cloudy, with uniform gradation and slight brightening towards the sun.
7	III	3	0.0	-1.0	5.0	-2.5	0.3	Partly cloudy, with a bright circumsolar effect and uniform gradation.
8	III	4	0.0	-1.0	10.	-3.0	0.45	Partly cloudy, rather uniform, with a clear solar corona.
9	IV	2	-1.0	-0.55	2.0	-1.5	0.15	Partly cloudy, with obscured sun.
10	IV	3	-1.0	-0.55	5.0	-2.5	0.3	Partly cloudy, with brighter circumsolar region
11	IV	4	-1.0	-0.55	10.0	-3.0	0.45	White–blue sky with distinct solar corona.
12	V	4	-1.0	-0.32	10.0	-3.0	0.45	CIE standard clear sky, low illuminance turbidity.
13	V	5	-1.0	-0.32	16.0	-3.0	0.3	CIE Standard clear sky, polluted atmosphere.
14	VI	5	-1.0	-0.15	16.0	-3.0	0.3	Cloudless turbid sky with broad solar corona.
15	VI	6	-1.0	-0.15	24.0	-2.8	0.15	White–blue turbid sky with broad solar corona.

3. METEOROLOGICAL DATA

The meteorological data used in this study have been collected at the radiometric station of the Public University of Navarra (UPNA, in its Spanish acronym), located on the rooftop of one of the buildings of the experimental farm of the School of Agricultural Engineering (42º47’32’’ N, 1º37’45’’ W, 435 m above sea level). Figure 2 shows the station’s location and the elevation angle of the visible horizon, which does not exceed 6º in any direction.

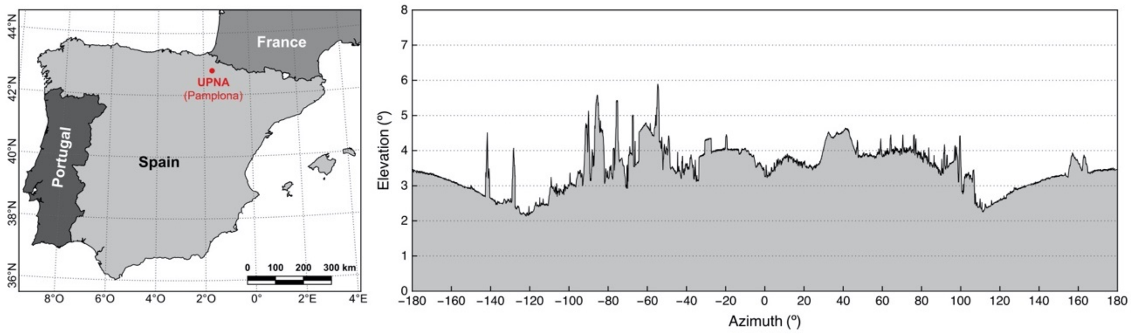

Figure 2. Situation of UPNA radiometric station (left) and diagram of the visible horizon (right).

The data used in this study were recorded from February 2008 to December 2013. During this period the following variables were measured at the UPNA radiometric station: global and diffuse horizontal irradiances, direct normal irradiance and radiance and luminance angular distribution in the sky vault. The global horizontal irradiance was measured by a Kipp & Zonen CM11 pyranometer. The diffuse horizontal irradiance was measured by a Kipp & Zonen CM11 pyranometer with shadow ball, whereas the direct normal irradiance was measured by a Kipp & Zonen CH1 pyrheliometer. The three instruments are mounted on a Kipp & Zonen 2 AP sun tracker.

The sky radiance and luminance angular distributions were measured at 10-min intervals by means of an EKO MS-321LR sky-scanner. This device is equipped with radiance and luminance sensors and spends more than 4 minutes to record the radiance and luminance values from the 145 patches in which the sky is divided following the CIE proposal (CIE, 1994). Sky-scanner sensors where calibrated by the manufacturer (EKO Instruments) in 2006, 2009 and 2011.

All records of irradiance, radiance and luminance for solar elevation angles lower than 5º have been discarded. The global, diffuse and direct irradiance data have been submitted to a quality control proposed within the framework of the MESoR project (Hoyer-Klick et al., 2008). This procedure raises three levels of quality control, that is, physical limits, clear-sky limits and redundancies. Those irradiance records (global, diffuse and direct) that did not pass the quality control have been rejected. Likewise, measurements of angular distribution of radiance and luminance corresponding to the discarded records due to the irradiance quality control have also been rejected.

Three criteria have been considered for the quality control of radiance and luminance measurements. Firstly, all records of individual sky patches exhibiting values out of the EKO sky-scanner measuring range (0-50 $kcd \cdot m^{-2}$ for luminance and 0-300 $W \cdot m^{-2} \cdot sr^{-1}$ for radiance) have been discarded. Likewise, all individual scans corresponding to sky sectors whose center is closer than 6º to the sun have also been discarded since the luminance and the radiance of the sun exceed the measuring range of the sky-scanner's sensors by several orders of magnitude. Therefore, when the sun is not covered by clouds or it is covered by thin clouds, the measurements corresponding to the sky patches closest to the sun can be saturated and provide erroneous records. Thirdly, all records whose integration on the horizontal plane deviates more than 30% from the measured diffuse irradiance in the same time period have been discarded in accordance to the quality-control test applied by Li et al. (2008) to radiance and luminance measurements.

For a more exhaustive quality control, it would have been necessary to integrate the luminance measurements and compare the result with the measured diffuse illuminance. However, during the period under consideration, the UPNA station did not have illuminance measurement instruments available. Thus, the luminance records have been considered valid whether the corresponding radiance records have passed the quality control. Therefore, while the radiance measurements have been subjected to the three levels of quality control, only the first two criteria could be applied to the luminance measurements.

Table II shows the result of the quality control for each of the years of the series of observations. As it can be seen, a total of 33322 records have passed the quality control tests. There are many months with no observations available. This is a consequence of the recurring technical problems suffered by the EKO sky-scanner during the period considered.

Table II. Number of measurements for each month and year of the observational time series.

	Month												
Year	Jan	Feb	Mar	Apr	May	Jun	Jul	Aug	Sep	Oct	Nov	Dic	Total
2007	0	89	757	544	711	720	823	1218	991	577	393	233	7056
2008	0	572	937	1398	1996	1940	1767	1572	1640	1301	1092	986	15201
2009	795	1119	1020	1018	1364	2109	0	0	0	0	0	0	7425
2010	0	0	0	0	0	0	0	0	0	0	21	456	477
2011	0	0	0	0	0	0	0	0	0	0	86	238	324
2012	46	201	136	271	153	190	108	67	151	135	200	101	1759
2013	159	55	113	183	182	186	60	52	47	30	5	8	1080
Total	1000	2036	2963	3414	4406	5145	2758	2909	2829	2043	1797	2022	33322

4. CLASSIFICATION METHODS

In this study, three different procedures for determining the ISO/CIE standard sky type have been used and evaluated. Two of them have already been proposed in other studies while the third one is a new approach. These methods are described below.

4.1. The method of relative gradation and indicatrix (RGI)

In this procedure, indicatrix and gradation functions corresponding to the sky under analysis are firstly identified by means of the analysis of relative luminance measurements, as it is described in Sections 4.1.1 and 4.1.2. Subsequently, the standard ISO/CIE sky type is obtained by combination of both functions (Section 4.1.3).

4.1.1. Determination of the indicatrix group

Considering Equation (1), if those measurements of the 145 ones recorded during each scan belonging to a certain almucantar (constant Z) are extracted, the ratio of the measured relative luminances ($L(Z,\gamma_i)/L_Z$) at different points on the same almucantar (which will have different χ) and that of a point for which χ = 90º (i.e., $L(Z,\gamma)_{\chi=90º}/L_Z$), will provide the successive points of the observed relative indicatrix function ($f(\chi_i)$), according to Equation (5).

$$\frac{\frac{L(Z,\gamma_i)}{L_Z}}{\frac{L(Z,\gamma)_{\chi=90º}}{L_Z}} = \frac{\frac{f(\chi_i)\cdot g(Z)}{f(Z_S)\cdot g(0)}}{\frac{f(90)\cdot g(Z)}{f(Z_S)\cdot g(0)}} = \frac{f(\chi_i)}{f(90)} = f(\chi_i). \tag{5}$$

The existence of a point with χ=90º on a given almucantar implies that the inequality of Equation (6) is verified.

$$\left|\frac{1}{\tan(Z)\cdot\tan(Z_S)}\right| \leq 1. \tag{6}$$

As an example, two almucantars are represented in Figure 3. On the almucantar 1 there are two points where χ=90, symmetrical to the solar meridian, whose azimuths meet Equation (7). In contrast, on the almucantar 2, there is no point where χ=90º since the maximum angular distance to the sun is lower than 90º.

$$(\gamma-\gamma_s) = \pm\cos^{-1}\left(\frac{1}{\tan(Z)\cdot\tan(Z_S)}\right). \tag{7}$$

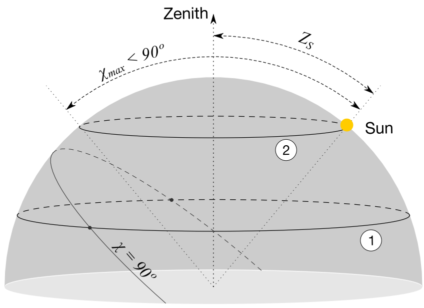

Figure 3. In this representation of the sky vault, two almucantars are shown, denoted as 1 and 2. Points with χ = 90º are also represented. On almucantar 1 there are two points where χ =90º. In contrast, there is no point with χ=90º on almucantar 2.

According to Equation (6), in case the almucantar corresponding to the sun elevation is chosen at a given moment, there will be points with χ=90º only when Z_S is higher than 45º. In case other almucantar is chosen to identify the indicatrix function, it must be taken into account that, as its zenith angle moves away from Z_S, the minimum distances to the sun increase. This causes a loss of information about the indicatrix function for small values of χ. In order to extend the observed indicatrix function to a wider range of χ

values, which will ensure a better identification of the indicatrix group, the following criteria have been adopted in this work:

- If $Z_S \geq 66$º, measurements corresponding to the closest almucantar to the solar one with $Z > Z_S$, from those collected in Table III, are used. This ensures that the range of χ extends from 6º to 132º. For example, if Z_S is equal to 70º, the measurements corresponding to the almucantar whose zenith angle is 72º are selected.
- If $Z_S < 66$º, measurements from two almucantars are used. The first one is the closest to the solar almucantar with $Z > Z_S$, among those presented in Table III, where points with χ=90º can be found. These measurements allow to define the experimental indicatrix function for small values of χ. The second almucantar is that of Z=78º. In this way, it is ensured, in the worst case (which corresponds to the solar noon of the summer solstice), that the experimental indicatrix function extends to values of χ ranging from 51 to 97º. According to Equation (5), there is no restriction to the joint use of the two aforementioned almucantars, provided that the luminances relative to the points where χ=90º on each almucantar are used.

Table III. Zenith angles of the considered almucantars in the determination of the indicatrix function and number of points corresponding to each of them.

Z (º)	12	18	24	30	36	42	48	54	60	66	72	78
Number of points in each almucantar, n_a	6	12	12	12	18	18	24	24	24	30	30	30

The position of the n_a points considered on each almucantar can be seen in Figure 4 represented by red dots. The assignment of experimental luminances to each of them is done as described below. On the almucantars with Z (12, 24, 36, 48, 60, 72, 84) they are assigned the value of the luminance observed by the sky-scanner in the corresponding sky patch. In the rest of the almucantars, the luminance assigned to its n_a points is the result of applying an Inverse Distance Weighting (IDW) interpolation of power 2 among the measurements of the sky-scanner in the closest patches (which can be two or three, as shown in Figure 4).

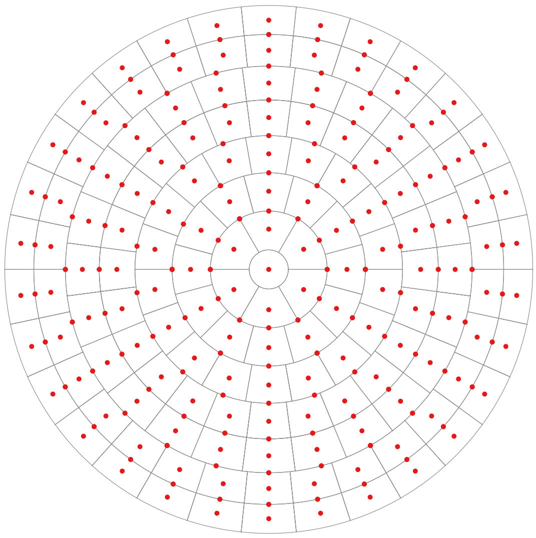

Figure 4. Position of the n_a points considered in each almucantar with respect to the CIE sky patches.

As it is highly probable that the points where χ=90º do not coincide exactly with any of the aforementioned n_a points, the luminances for χ=90º, on each side of the solar meridian ($L_{1(\chi=90º)}$ and $L_{2(\chi=90º)}$), are obtained by averaging the luminances corresponding to the closest two n_a points on each side. The ratios of luminances $L(Z, \gamma_i)$ on each side of the solar meridian to the corresponding $L_{1(\chi=90º)}$ or $L_{2(\chi=90º)}$ are the values $f(\chi_i)$ of the experimental indicatrix function.

Subsequently, the RMSD between the experimental indicatrix function values and those corresponding to each of the six standard indicatrix functions is calculated. The standard indicatrix group exhibiting the lowest RMSD is assigned to the sky under study. At the end of the process three groups of indicatrix functions are identified for each sky scan, one for each side of the solar meridian and a third one for the whole sky, as it was already done by Kómar et al. (2013) from measurements made by a portable spectral sky-scanner.

4.1.2. Determination of the gradation group

The relative luminances of interest are those corresponding to the points with a constant distance to the sun (χ). At these points the indicatrix function remains constant and the luminance variation that can be observed is only attributable to the gradation function. For a given χ, these points are located in the circumference that results from the intersection of the sky vault and a cone whose vertex is in the center of said vault, its axis follows the sun vector direction and has an opening angle of χ (see Figure 5). If an angular distance to the sun is chosen which satisfies $\chi = Z_S$, Equation (1) is reduced to Equation (8). Therefore, the observed luminance relative to the zenith in the successive Z_i provides the values of the experimental relative gradation function.

$$\frac{L(Z,\gamma)_{\chi=Z_S}}{L_Z} = \frac{f(Z_S) \cdot g(Z)}{f(Z_S) \cdot g(0)} = \frac{g(Z)}{g(0)}. \tag{8}$$

It can be seen in Figure 5 that if $Z_S > 45º$, when taking the luminances of the points where $\chi = Z_S$, the complete experimental gradation function can be described from Z = 0 to Z = 90º. In contrast, if $Z_S < 45º$ the information from the lower almucantars is lost. In this case, the comparison among the experimental gradation function and the standard ones is less accurate. For this reason, the following criteria have been adopted in this work:

- If $Z_S > 45º$, the experimental values corresponding to the distance to the sun $\chi = Z_S$ are considered (see Figure 5a).
- If $Z_S < 45º$, the experimental luminance values at two different distances to the sun are considered. The first one is equal to Z_S and the second one is equal to 90º, as already proposed by Kittler (1985) (see Figure 5b). In this case, for χ = 90º, Equation (1) becomes Equation (9). Unlike what happens when $\chi = Z_S$, the luminance values relative to the zenith do not provide the relative gradation function values. To obtain $f(Z_S)$ it is enough to divide the luminance values

relative to the zenith for the same Z in the two circles represented in Figure 5b, as described in Equation (10). The successive values of the experimental gradation function are those corresponding to $\chi = Z_S$ plus those corresponding to χ = 90º multiplied by $f(Z_s)$.

$$\frac{L(Z,\gamma)_{\chi=90º}}{L_Z} = \frac{f(90º)\cdot g(Z)}{f(Z_S)\cdot g(0)} = \frac{g(Z)}{f(Z_S)\cdot g(0)}. \tag{9}$$

$$f(Z_S) = \frac{L(Z,\gamma)_{\chi=Z_S}}{L(Z,\gamma)_{\chi=90º}}. \tag{10}$$

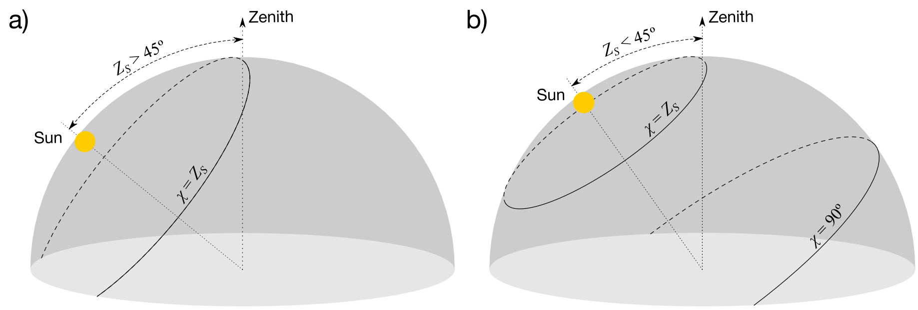

Figure 5. When $Z_S > 45º$, the line defined by the points with $\chi = Z_S$ sweeps all sky almucantars (a). When $Z_S < 45º$, such line is not enough to cover the lower almucantars. Therefore, it is necessary to include the line defined by the points with $\chi = 90º$ (b).

For the assignment of the experimental luminance to a certain point, an IDW interpolation is applied among the four sky-scanner measurements corresponding to the closest sky patches. As in the case of the indicatrix function, the assigned standard gradation group is the one with the lowest RMSD in relation to the experimental values. Again, this analysis has been carried out separately on both sides of the solar meridian and jointly. So, at the end of the process, three gradation groups are identified for each sky scan, one for each side of the solar meridian, and the third for the whole sky.

4.1.3. Determination of the ISO/CIE sky according to the gradation and indicatrix groups

By combining the six gradation groups with the six indicatrix groups, it would be possible to identify up to 36 different sky types. However, only 15 of all possible combinations are considered as standards by CIE. In this sense, Dumortier and Kobav (2007) proposed a reduction from 36 sky types to 15 ISO/CIE standard sky types (Table IV). For this, 36 sky luminance distributions were calculated for 5181 sky elements for each sky type. This sky elements resulted from an equisolid angle grid defined with an altitude every 2º. Non-standardized sky luminance distributions were compared with each of the standard skies. The sky type with the lowest RMSD was considered equivalent to an ISO/CIE sky type. The results of this analysis were specified in a single reduction table suitable for any solar elevation (see Table IV). This proposal was used by Kobav et al. (2012) for the characterization, according to the ISO/CIE standard, of sky-scanner measurements made at the IDMP station in Lyon (France).

Table IV. Matrix with 15 ISO/CIE standard sky types sorted according to gradation and indicatrix combination (Kobav et al., 2012).

Indicatrix	Gradation					
	I	II	III	IV	V	VI
1	1	3	5	9	9	9
2	2	4	6	9	9	9
3	2	7	7	10	10	12
4	8	8	8	11	12	14
5	8	8	8	11	13	14
6	8	8	8	13	13	15

Combinations of gradation and indicatrix shown in Table IV are reviewed in this work. Again, 36 sky-luminance distributions are generated considering 71158 sky elements in each type. This sky division is explained in more detail in Section 4.3. Each of the non-standardized distributions is compared with the 15 standard types. As in the proposal of Dumortier and Kobav (2007), the sky type with the lowest RMSD is considered to be equivalent to a ISO/CIE sky type. This analysis is repeated considering solar elevations from 1º to 90º. It has been found that the assignment of non-standard sky types to standard ones varies with solar elevation. Therefore, a set of reduction tables dependent on the solar elevation is generated in sun altitude intervals of 1º. This issue is further addressed in Section 5.4.

4.2. The method of normalized luminances (NL)

In this procedure, proposed by Tregenza (2004), the relative luminance distribution measured on the 145 sky patches, according to CIE (1994), is compared with the relative luminance distribution corresponding to each of the 15 CIE Standard General Sky types. The standard type assigned to each moment is the one exhibiting the lowest RMSD between the measured and standardized luminances. The steps described below are followed:

- Calculation of D_v considering the measured luminance distribution, according to Equation (11).

$$D_v = F_c \sum_p D_{vp}, \tag{11}$$

  where F_c is a correction factor and D_{vp} is the horizontal diffuse illuminance coming from sky patch p, calculated by Equation (12).

$$D_{vp} = \int_{\alpha_1}^{\alpha_2} \int_{\gamma_1}^{\gamma_2} L_p \sin\alpha \cos\alpha \, d\alpha d\gamma = \left(L_p/2\right)(\sin^2\alpha_2 - \sin^2\alpha_1)(\gamma_2 - \gamma_1), \tag{12}$$

  where α_1, α_2 and γ_1, γ_2 are, respectively, the elevation angles above the horizon and azimuths delimiting the sky patch p.

  The 145 patches are grouped in 8 bands (b_p) described in Table V and the geometrical factor (F_g) of the different patches is calculated by Equation (13).

$$\begin{gathered} F_g = \left(\pi/n_{pb}\right)\left[\sin^2\left(b_p\pi/15\right)\right] - \sin^2\left[\left(b_p - 1\right)\pi/15\right] \text{ for } 1 \leq b_p \leq 7, \\ F_g = \pi\left[1 - \sin^2(7\pi/15)\right] \text{ for } b_p = 8, \end{gathered} \tag{13}$$

  where n_{pb} is the number of patches in each band b_p.

Table V. CIE sky patches distribution.

Band, b_p	Patches, p	Elevation of the band center (º)	Number of patches in band, n_{pb}
1	1-30	6	30
2	31-60	18	30
3	61-84	30	24
4	85-108	42	24
5	109-126	54	18
6	127-138	66	12
7	139-144	78	6
8	145	90	1

The correction factor (F_c) is calculated by Equation (14).

$$F_c = \pi / S_d, \tag{14}$$

where S_d is the result of the summation in Equation (15), which corresponds to the patches really considered in each scan.

$$S_d = \sum_p F_{gp} \,. \tag{15}$$

- Division of the luminance corresponding to each scan (L_p) by the calculated horizontal illuminance, as indicated in Equation (16). The observed normalized luminance distribution (L_{pn}) is obtained for each scan. This distribution is later compared with the one given for each standard sky.

$$L_{pn} = L_p / D_v. \tag{16}$$

- Calculation of the zenith relative luminance distribution for each standard general sky type, for the same time as the corresponding to the recorded scans. For doing so, Equation (17), which is derived from Equation (1), is applied to obtain the zenith relative luminance (l) corresponding to a point in the sky with coordinates (Z, γ). Coefficients a, b, c, d and e depend on the standard general sky type, in accordance with Table I.

$$l(Z,\gamma) = \frac{\{1 + c[\exp(d\chi) - \exp(d\pi/2)] - e\cos^2\chi\}[1 + a\exp(b/\cos Z)]}{\{1 + c[\exp(dZ_S) - \exp(d\pi/2)] - e\cos^2 Z_s\}[1 + a\exp(b)]}. \tag{17}$$

In the first 144 patches, Equation (17) is applied to the four vertices and the resulting average luminance relative to zenith ($l_{p,st}$) is assigned to the corresponding patch. In the patch 145, the luminance is obtained by averaging the values calculated for each of the six equilateral triangles in which the patch is divided, as proposed by Tregenza (2004).

- Division of the calculated luminances for each scan and standard sky type by the corresponding horizontal illuminance. Firstly, Equations (11), (13) and (14) are applied to the luminances obtained by Equation (17) during each scan. This way, the horizontal zenith relative illuminances corresponding to each of the standard skies are obtained. Secondly, a normalization process is conducted. By applying the equation equivalent to Equation (16), the normalized luminances ($L_{pn,st}$) are obtained in each patch, for each sky type and scan.
- Calculation of RMSD values between each standard sky type and the measured values. For each scan, the RMSDs are calculated considering the measured normalized luminances and the 15 luminance distributions, corresponding to the standard sky types, according to Equation (18).

$$RMSD_{st} = \sqrt{\frac{1}{n_p}\sum_{n_p}\left(L_{pn} - L_{pn,st}\right)^2}, \tag{18}$$

where n_p is the total number of sky patches considered.

- Selection of the standard sky type. The selected standard sky type is the one exhibiting the lowest RMSD out of 15 types calculated in the previous step.

This procedure has been applied to the entire sky vault and to each of the two halves of the sky separated by the solar meridian. This way, at the end of the process, 3 sky types are identified for each scan, one for each of the divisions created by the solar meridian, and the third one for the whole sky.

4.3. The method of relative zenith luminances (RZL)

This procedure is based on the method described in Section 4.1.3 for the assignment of non-standardized gradation and indicatrix function combinations to the 15 ISO/CIE standard skies. In this method, in contrast to the two already described, only the sky regions measured by the sky-scanner are considered when comparing the measured and modeled values of luminance. For example, the NL method uses the luminance value of the four vertices of the sky patch defined by the CIE to obtain the average luminance for each of the 145 CIE patches. However, the field of view (FOV) of the sky-scanner causes the measured sky area to be circumscribed to said patch (see Figure 6), so that none of the four vertices is measured by the sky-scanner.

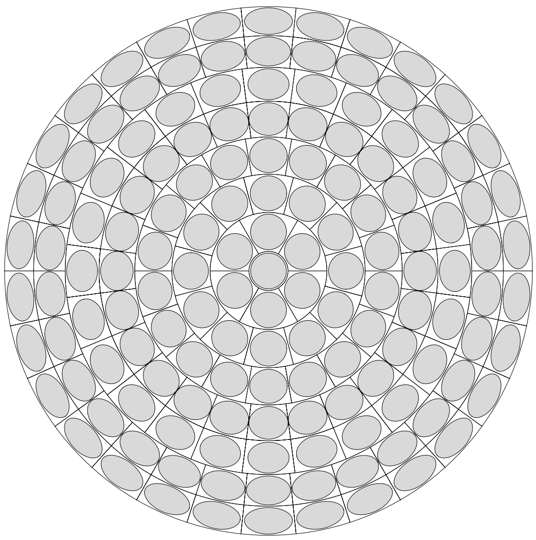

Figure 6. Subdivision of the sky vault into 145 patches according to CIE (1994) (black polygons) and sky elements measured by the EKO sky-scanner with 11º FOV (gray-shaded ellipses and circles).

The new proposed method comprises the following steps:

- Definition of a square grid within which the projection of the sky vault on the horizontal plane is inscribed. In this work a square grid of 301 x 301 cells is used. These dimensions can be adjusted according to the needs of the subsequent study.
- Determination of the zenith angle (Z) and azimuth (γ) corresponding to the center of each of the grid cells assuming an equisolid projection. Any other projection

can also be employed; however, the use of the equisolid has a distinct advantage from the point of view of a possible integration of the cells' luminance values, since all cells of the matrix have the same solid angle. In this way, it is possible to generate an image (of 301 x 301 pixels in this particular case) whose pixels are defined by the zenith angle and the azimuth of their center. However, only 71158 pixels out of 90601 that make up the square image correspond to the sky projection. Equation (19) relates the projected distance between a pixel and the center of the image (R) and the corresponding zenith angle (Z) according to an equisolid projection.

$$R = 2 \cdot \sin(Z/2). \quad (19)$$

- At a given time, when the sun position is defined by its zenith angle (Z_S) and azimuth (γ_S), an angular distribution image of luminance relative to the zenith for each of the 15 ISO/CIE standard skies is generated. To do this, Equation (17) is applied to each of the pixels of the image. Figure 7 shows an example of the obtained distributions for each of the 15 ISO/CIE standard considering a solar zenith angle of 60º at solar noon.

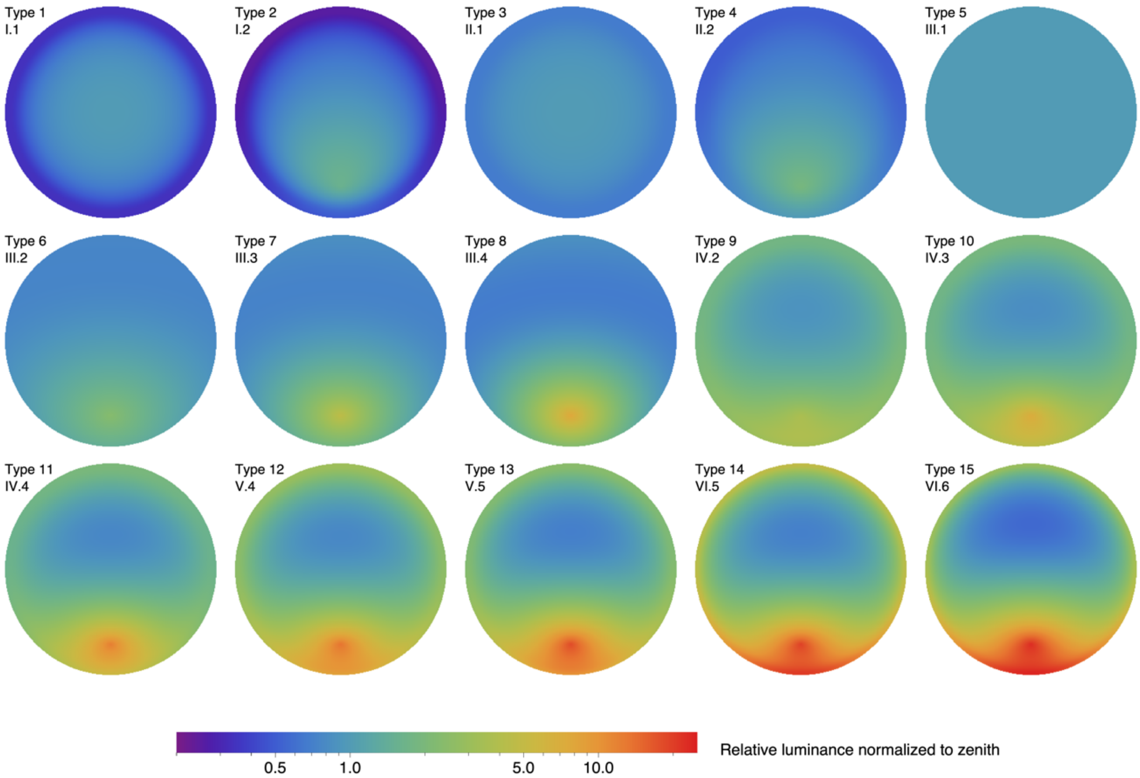

Figure 7. Angular distribution of sky luminances for each of the 15 ISO/CIE standard sky types.

- For each of the 15 images generated in the previous step, there is calculated the mean relative luminance corresponding to each of the 145 sky patches defined by CIE ($l_{p,st}$) by averaging the relative luminances corresponding to the internal cells of the patch in question. For this, it is considered the FOV of the sky-scanner used to measure the angular distribution (11º in the case of the EKO sky-scanner). Figure 8 shows, for each of the 15 standard distributions represented in Figure 7, the relative luminances corresponding to the sky elements measured by the sky-scanner.

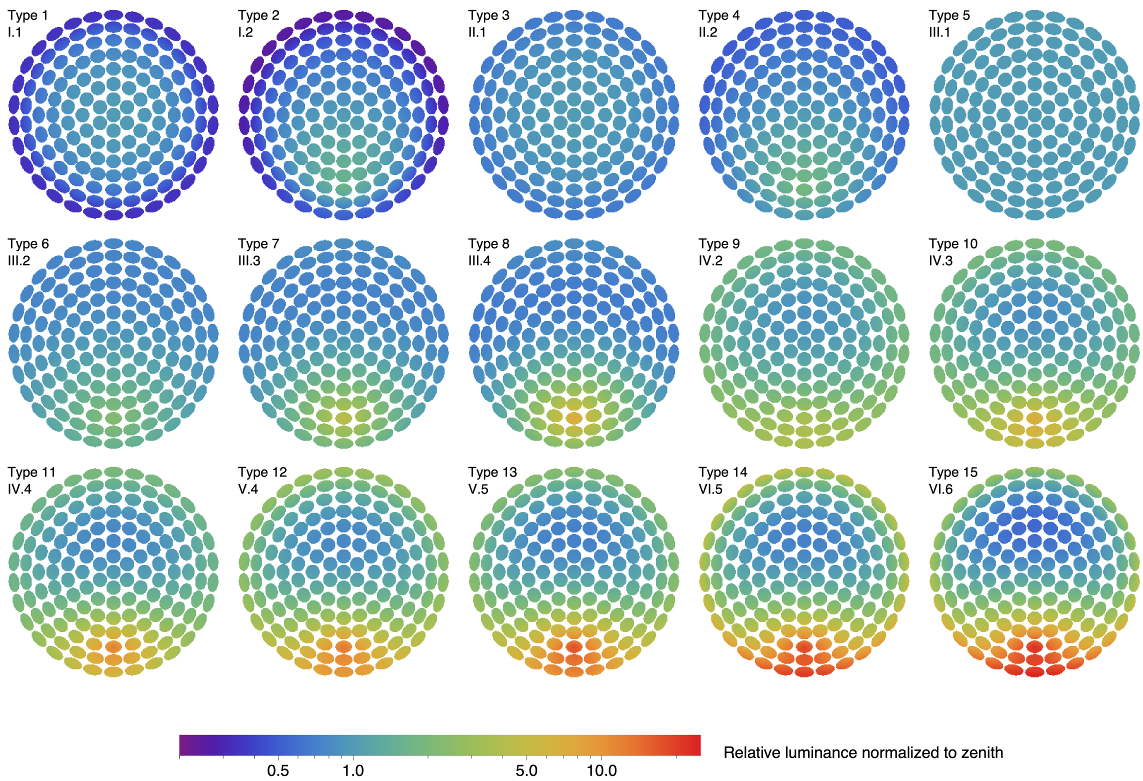

Figure 8. Sky elements measured by the sky-scanner for each of the 15 standard luminance distributions represented in Figure 7.

- Comparison of the angular distribution values of luminance relative to the zenith luminance measured by the sky-scanner (l_p) with the modeled values corresponding to each of the 15 standard skies ($l_{p,st}$). To do so, the RMSD is calculated using Equation (20). In general, the number of sectors considered (n_p) will be lower than 145 since luminance data have been previously submitted to a quality control that discards those sectors that do not meet the established criteria.

$$RMSD_{st} = \sqrt{\frac{1}{n_p}\sum_{n_p}\left(l_p - l_{p,st}\right)^2}. \quad (20)$$

- The selected standard sky type is the one out of the 15 calculated in the previous step that exhibits the lowest RMSD.

As in the two procedures described above, this method has been applied to the whole sky and to each half of the sky resulting from its division by the solar meridian. So, three sky types have been determined from each measurement made by the sky-scanner.

5. RESULTS AND DISCUSSION

The three methods described were applied to the series of radiance and luminance sky-scanner measurements. The classification algorithms were developed in Wolfram Mathematica and run in the Computing Cluster of UPNA Research Institutes. The different results obtained are presented and analyzed in the following subsections.

5.1. Comparison of ISO/CIE standard sky types obtained from luminance and radiance measurements

The coincidences between the sky types obtained by the NL method from luminance measurements and those obtained from radiance measurements are represented in Figure 9a. It can be seen that most coincidences are grouped around the diagonal of the graph, which indicates that there is a good agreement between both classifications.

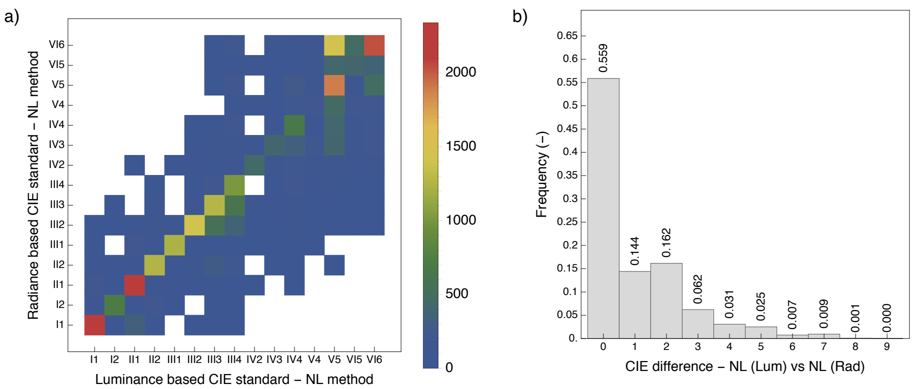

Figure 9. (a) Coincidence matrix of standard sky types obtained by the NL method from luminance and radiance measurements. The colored scale corresponds to the number of cases referring to the same sky type. (b) Frequency distribution of differences among the sky types obtained from luminance and radiance measurements.

The histogram in Figure 9b quantifies this trend. It shows the frequency distribution of the differences between the sky types obtained from luminance and radiance measurements. The matches in ISO/CIE standard classification are 55.9%. The cases in which the gap has a difference of 1 or 2 types are 14.4% and 16.2%, respectively, and fall significantly after this difference. That is, in 86.5% of the cases, the ISO/CIE standard sky obtained differs at most by 2 types when classifying from luminance and radiance measurements by the NL method. Examining the tail of the histogram, it can also be seen that there are no classification gaps higher than 8 types.

The results with the RGI method are similar to those obtained with the NL one (see Figure 10). Again, agreements are grouped around the diagonal of the coincidence diagram is shown in Figure 10a. In this case, the frequency of coincidence between the two classifications rises slightly (up to 58.3%) as can be seen in Figure 10b. The cases in which the difference between the sky types obtained from luminance and radiance amounts to 1 and 2 sky types are 19.3% and 12.8%, respectively. So, in this case, in 90.4% of the cases the classifications deviate less than 2 types.

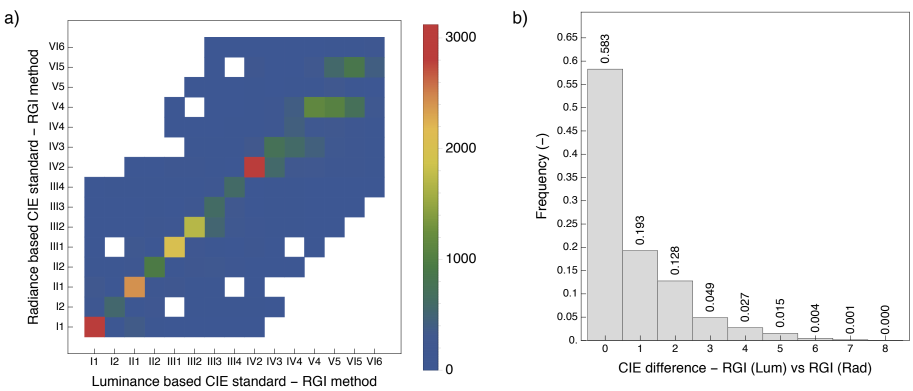

Figure 10. (a) Coincidence matrix of standard sky types obtained by the RGI method from luminance and radiance measurements. The colored scale corresponds to the number of cases referring to the same sky type. (b) Frequency distribution of differences between the sky types obtained from luminance and radiance measurements.

The trend in the case of the RZL method when using luminance and radiance measurements is maintained. It can again be seen that the coincidences among equal standard skies are concentrated in the diagonal of the coincidence diagram (see Figure 11a). In this case, the number of exact matches amounts to 58.9% (see Figure 11b). If, as in the two previous cases, the frequencies corresponding to differences of 1 or 2 sky types are considered, the coincidences reach 87.3%.

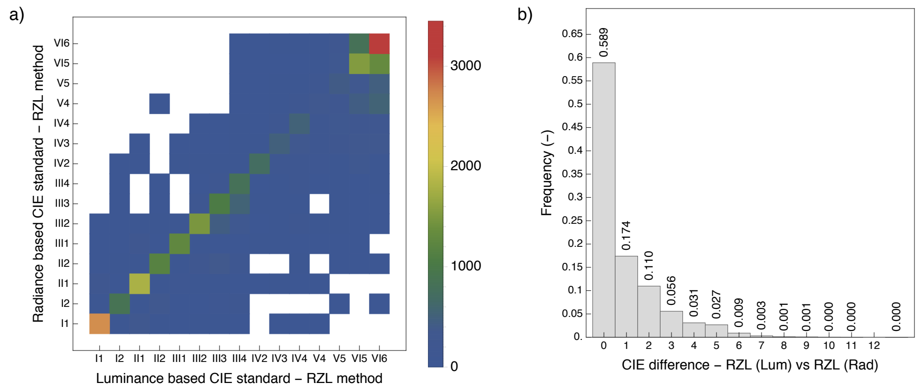

Figure 11. (a) Coincidence matrix of standard sky types obtained by the RZL method from luminance and radiance measurements. The colored scale corresponds to the number of cases referring to the same sky type. (b) Frequency distribution of differences between the sky types obtained from luminance and radiance measurements.

5.2. Comparison of classification procedures considering the 15 ISO/CIE standard sky types

In this section, the analysis of the resulting coincidences is presented when classifying the skies according to the CIE standard with the three methods described in Section 4.

Figures 12a and 12c show the coincidence diagrams obtained when classifying the skies with the NL and RZL methods, respectively. In both cases, it is observed that the greatest number of coincidences is grouped around the diagonal in each diagram. In the case of the luminance-based classification, exact matches (same ISO/CIE standard) account for 45.6% of the cases (see Figure 12b). When classifying with radiance measurements, the agreement reaches 49.2%, as can be seen in Figure 12d.

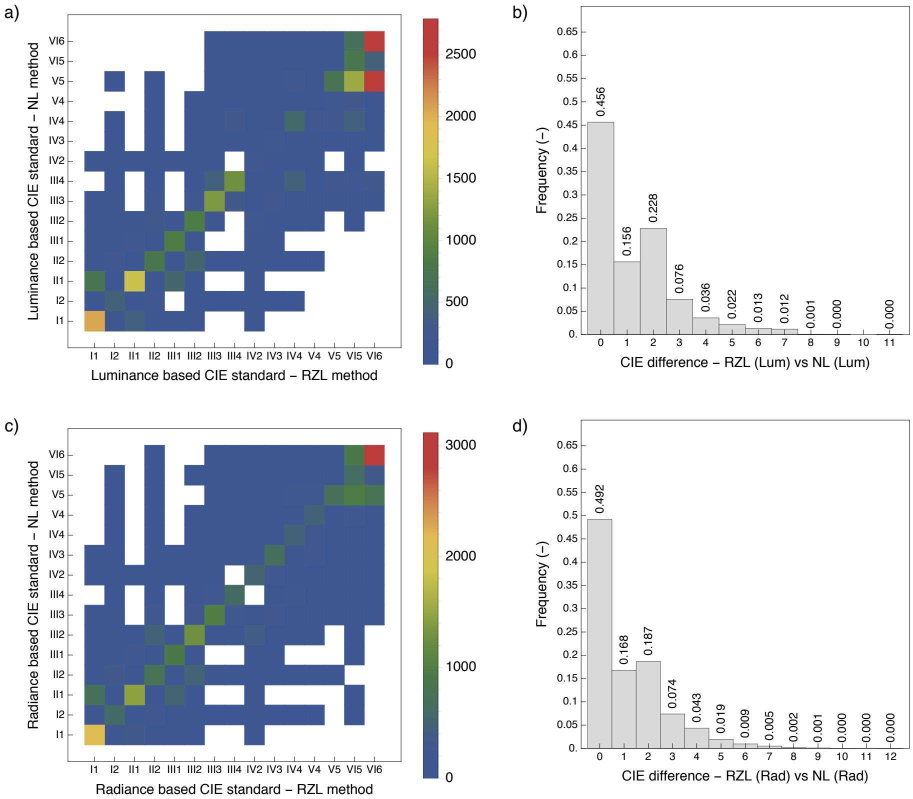

Figure 12. Coincidence matrix of standard sky types obtained by the NL and RZL methods from luminance (a) and radiance measurements (c); the colored scale corresponds to the number of cases referring to the same sky type. Frequency distribution of differences among the sky types obtained by the NL and RZL methods from luminance (b) and radiance measurements (d).

Figure 13 shows the comparisons between the standard skies obtained by applying the NL and the RGI methods. When analyzing the coincidence diagrams corresponding to the classification with luminances and radiances (Figures 13a and 13c, respectively), a greater dispersion of the exact matches is observed, especially in the clearest types of sky. This results in a frequency of coincidences of 27% in the case of the classification based on luminance and 23.9% for the radiance. In the particular case of the classification based on radiance measurements, it is observed that the frequency gap of one ISO/CIE standard is greater than the frequency of exact coincidences.

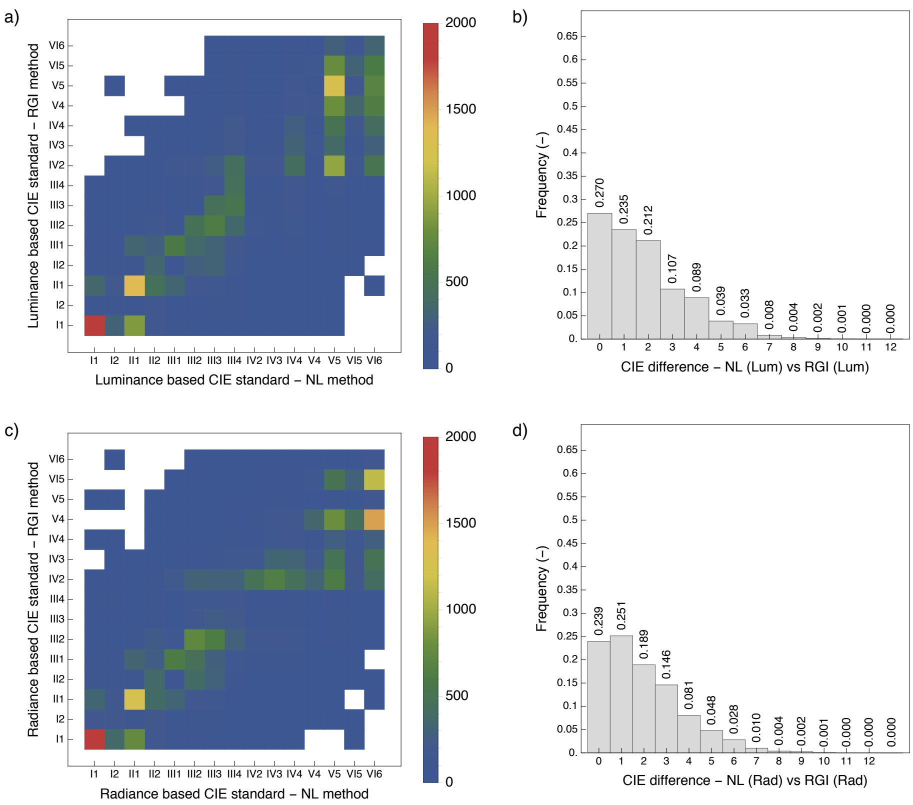

Figure 13. Coincidence matrix of standard sky types obtained by the NL and RGI methods from luminance (a) and radiance measurements (c); the colored scale corresponds to the number of cases referring to the same sky type. Frequency distribution of differences among the sky types obtained by the NL and RGI methods from luminance (b) and radiance measurements (d).

Figure 14 shows the comparisons among the standard skies obtained by the RZL and the RGI methods. As in the previous case, there is a certain concentration of coincidences around the diagonal in Figures 14a and 14c, corresponding to the classifications based on luminance and radiance measurements. A frequency of exact matches of around 30% is seen in both cases when the histograms for each type of measurements are analyzed.

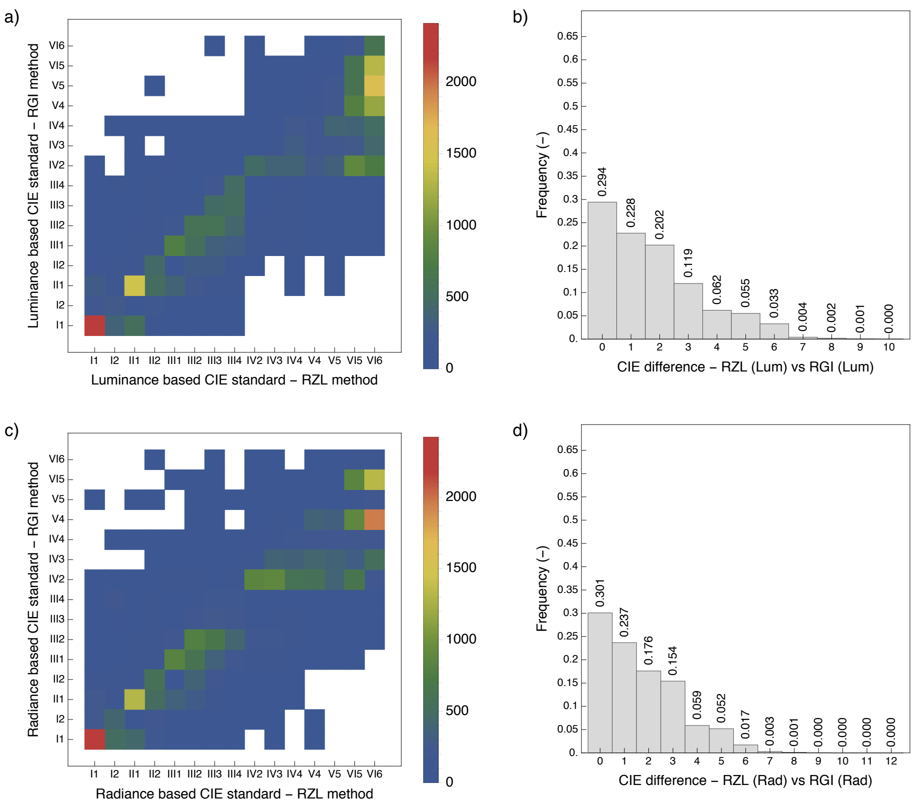

Figure 14. Coincidence matrix of standard sky types obtained by the RZL and RGI methods from luminance (a) and radiance measurements (c); the colored scale corresponds to the number of referring to the same sky type. Frequency distribution of differences among the sky types obtained by the RZL and RGI methods from luminance (b) and radiance measurements (d).

5.3. Analysis of sky classification symmetry

The analysis of the sky-classification symmetry gives an idea of its homogeneity. It must be noted that all standard skies defined by ISO/CIE, whether overcast, intermediate or clear, are homogeneous skies. This is because gradation and indicatrix standard functions are analytically defined functions.

In this section the symmetry in the sky classification is analyzed. As explained in Section 4, apart from classifying the whole sky by the three methods, the two sky halves on each side of the solar meridian have also been classified. So, from now on, those skies in which the classification in both sides of the solar meridian coincide will be called symmetrical skies.

Figure 15a shows the coincidences frequency among the types obtained from each half of the sky by the NL method. It can be observed that 37.6% are symmetrical skies, that is, in 37.6% of the cases the ISO/CIE standard sky on one side of the sky coincides with the other side and, therefore, with the global sky classification. Figure 15b shows the symmetry frequencies obtained for each standard sky type with the NL method. The type of sky with a higher proportion of symmetrical skies is I1 (CIE Standard Overcast Sky), whereas VI5 (cloudless turbid sky with broad solar corona) exhibits the lowest frequency in symmetrical skies.

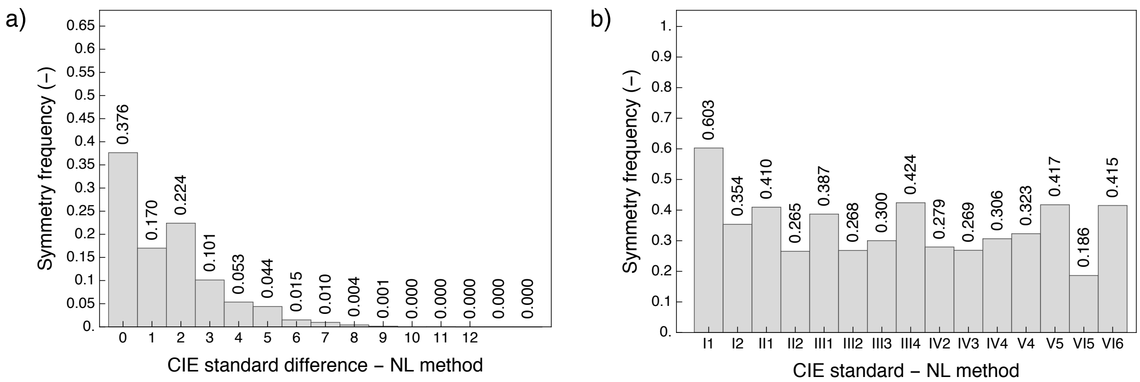

Figure 15. (a) Frequency distribution of coincidences between the standard sky types obtained from each of the two sky halves divided by the solar meridian with the NL method. (b) Symmetry frequencies obtained for each standard sky type.

Figure 16 shows the symmetry results obtained with the RGI method. In this case, the frequency of symmetric skies is similar to that obtained with the NL method, reaching a value of 38.9%. However, when analyzing the frequency of symmetric skies by type, a somewhat different distribution is appreciated. Again, the type with the highest frequency of symmetric skies is I1, closely followed by IV2 type (partly cloudy, with obscured sun).

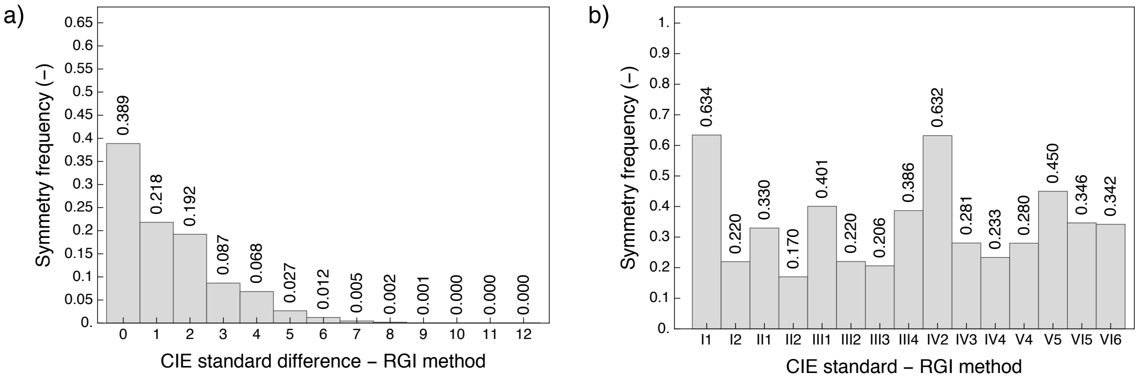

Figure 16. (a) Frequency distribution of coincidences between the standard sky types obtained from each of the two sky halves divided by the solar meridian with the RGI method. (b) Symmetry frequencies obtained for each standard sky type.

When analyzing the symmetry of the skies classified by the RZL method the frequencies increase. Considering all sky types globally, there are 57% symmetric skies, as shown in Figure 17a. If the results are analyzed by ISO/CIE standard type, it can be observed that types I1 and VI6 (white-blue turbid sky with broad solar corona) exceed 70% of symmetric skies (see Figure 17b).

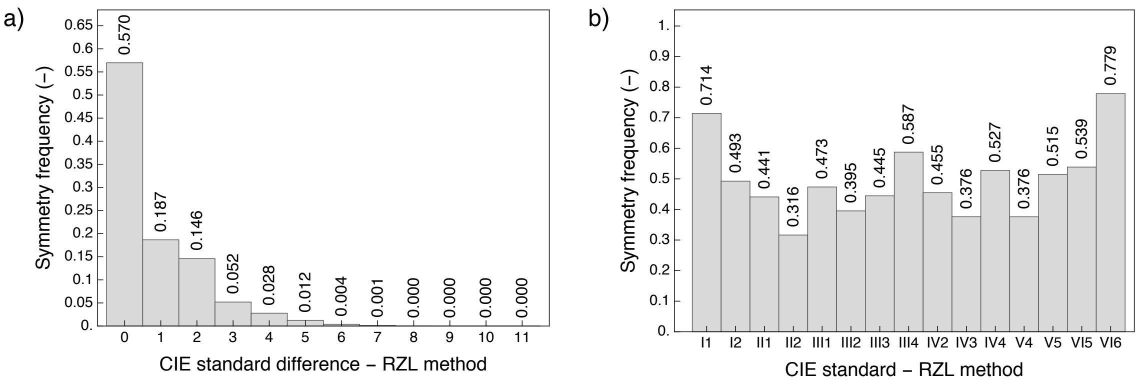

Figure 17. (a) Frequency distribution of coincidences between the standard sky types obtained from each of the two sky halves divided by the solar meridian with the RZL method. (b) Symmetry frequencies obtained for each standard sky type.

5.4. Assignment of the non-standardized combinations of the indicatrix gradation functions to the CIE standard sky types

Section 4.1.3 mentioned the proposal of Dumortier and Kobav (2007) for the assignment of non-standardized combinations of gradation and indicatrix functions to the ISO/CIE standard sky types. The initial proposal by these authors suggests a unique reduction table suitable for all solar elevations (see Table IV). In this work a set of reduction tables dependent on solar elevation (from 1 to 90 degrees) is proposed. For reasons of space, it is not possible to include the obtained 90 tables in the present work.

In order to compare Dumortier and Kobav's proposal with the revision carried out in this study, the sky classification obtained from both proposals by the RGI method has been compared, observing an agreement of 88% of the cases (see Figure 18). Only luminance has been considered.

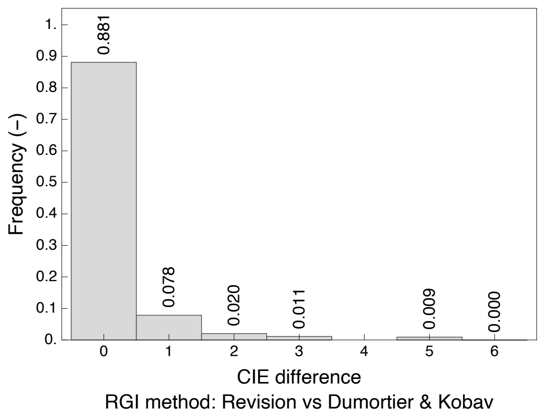

Figure 18. Coincidence frequency distribution among the standard sky types obtained by the RGI method when comparing the Dumortier and Kobav's proposal (Dumortier and Kobav, 2007) and the new assignment carried out considering the solar elevation.

Sky classifications obtained by applying each of the two proposals for assigning ISO/CIE standard skies from the gradation and indicatrix functions to resulting sky types with NL and RZL methods are compared. Figure 19a shows the coincidence frequencies obtained by the NL and RGI methods considering the revision of the standard skies' assignment. The frequency of exact matches is 26.8%. On the other hand, Figure 19b shows the coincidence frequencies of the sky types obtained by the NL and the RGI methods considering the Dumortier and Kobav's proposal. The frequency of exact matches in this case is practically the same as in the previous case.

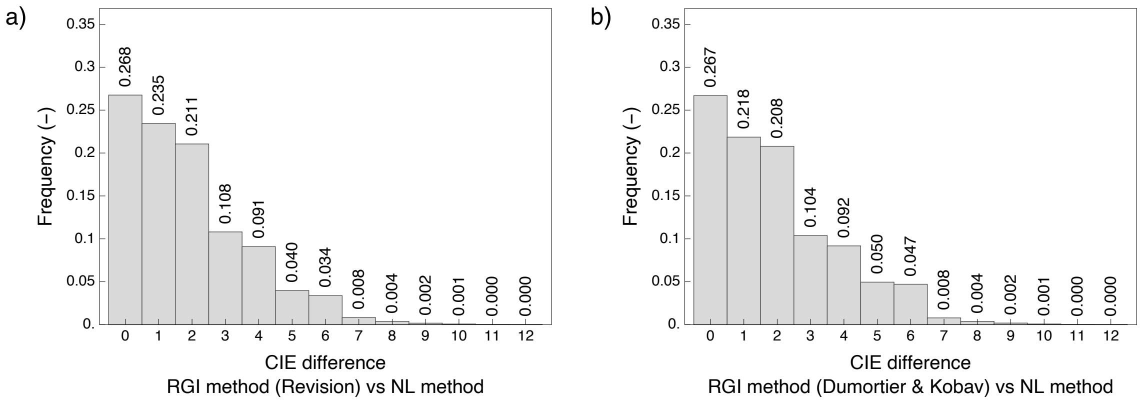

Figure 19. Frequency distribution of differences among the standard sky types obtained by the NL and RGI methods when considering (a) the revision carried out and (b) the Dumortier and Kobav's proposal (Dumortier and Kobav, 2007).

When making the same comparison with the results obtained by the RZL method (see Figure 20a), the frequencies distribution pattern observed in the previous case with the NL method is maintained here too. The proportion of exact matches when applying the revision (29.1%) slightly exceeds that obtained when applying the initial proposal (28.6%), as can be seen in Figure 20b.

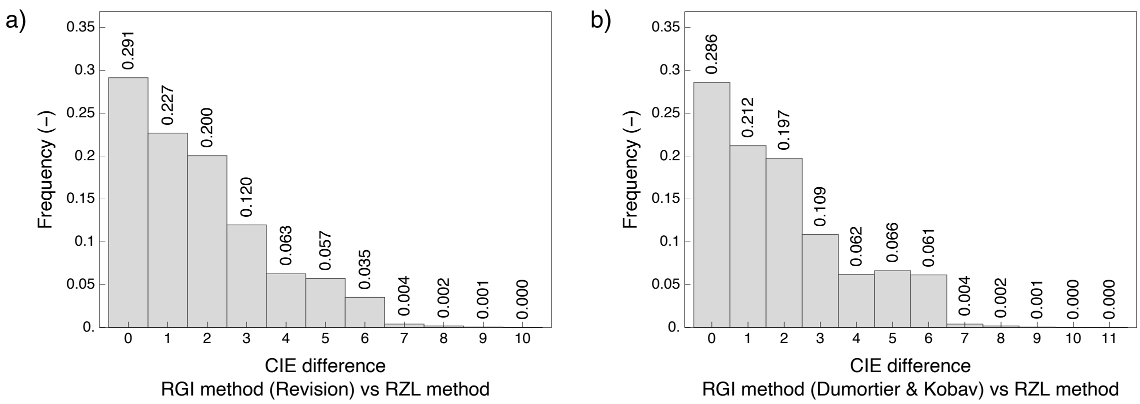

Figure 20. Frequency distribution of differences among the standard sky types obtained by the RZL and RGI methods when considering (a) the revision carried out and (b) the Dumortier and Kobav's proposal (Dumortier and Kobav, 2007).

6. CONCLUSIONS

This work analyzed the existing differences in the characterization of the sky conditions according to the CIE Standard General Sky comparing the results obtained with three classification procedures. Although the ISO/CIE standard skies are based on photometric variables, the possibility of classifying the skies from radiance, instead of luminance, was also studied. Likewise, the obtained differences in the resulting sky type when classifying the two parts of the sky separated by the solar meridian have been compared. In general terms, it is possible to conclude that there are certain differences in the classification whose magnitude depends on the applied method to characterize the sky.

In the absence of a reference case, it is not possible to establish which procedure performs best in absolute terms. For this reason, the three proposed methods have been compared in pairs. This analysis revealed that the RZL method was the one that performed best since it exhibited the highest number of coinciding sky types with those obtained by the NL and RGI methods. Specifically, the two methods that showed the best agreement were the NL and RZL ones. This is not surprisingly since, apart from the peculiarities explained above, the RZL method is an evolution with higher resolution of the NL one. In contrast, the methods that exhibited the worst result were the pair NL - RGI. The differences in the classification as a consequence of the applied methods has been evidenced at this point since the frequency of coincidences among the sky types obtained ranged between 49% for the pair NL - RZL and 24% when NL and RGI methods were compared.

When comparing the standard sky types obtained from radiance and luminance measurements, there has been observed that the coincidence for the standard sky types ranges from 55% to 59%. The RZL method reached the greatest agreement among the types obtained from both variables. When in addition to the matching sky types, the differences of 1 and 2 sky types were considered, the coincidence frequency approached 90%. Therefore, given these limitations and in the absence of luminance data, classification can be made from sky-radiance measurements.

Symmetric skies have been defined as those in which the classification of the two parts of the sky separated by the solar meridian coincide and, therefore, are equal to the global classification. In this sense, whereas the frequency of symmetrical skies identified by the NL and RGI methods is similar, around 38-39%, the proportion of symmetric skies classified by RZL amounts to 57%. Therefore, it can be concluded that the sky symmetry is also very sensitive to the method used.

Finally, the sensitivity of the obtained sky type frequencies has been analyzed depending on the proposal used for allocating the non-standardized combinations of indicatrix and gradation functions to the ISO/CIE standard types. In this sense, two proposals have been compared, that of Dumortier and Kobav (2007) and a proposal in the present study. The consequences of the application of any of the two reduction proposals are not very significant, as an 88% agreement has been observed between both classifications.

ACKNOWLEDGMENTS

This work was performed in the framework of Project IRILURREFLEX (ENE2017-86974-R), financed by the Spanish State Research Agency (Agencia Estatal de Investigación, AEI) and European Regional Development Fund (Fondo Europeo de Desarrollo Regional, FEDER). The authors would like to thank the Public University of Navarre for awarding Ignacio García Ruiz a Doctoral Fellowship and the reviewers for their useful comments and suggestions.

REFERENCES

Bartzokas, A., Kambezidis, H.D., Darula, S., Kittler, R., 2003. Sky luminance distribution in Central Europe and the Mediterranean area during the winter period. J. Atmos. Solar-Terrestrial Phys. 65, 113–119. https://doi.org/10.1016/S1364-6826(02)00283-3

Bartzokas, A., Kambezidis, H.D., Darula, S., Kittler, R., 2005. Comparison between winter and summer sky-luminance distribution in Central Europe and in the Eastern Mediterranean. J. Atmos. Solar-Terrestrial Phys. 67, 709–718. https://doi.org/10.1016/J.JASTP.2004.12.008

Brunger, A.P., Hooper, F.C., 1993. Anisotropic sky radiance model based on narrow field of view measurements of shortwave radiance. Sol. Energy 51, 53–64. https://doi.org/10.1016/0038-092X(93)90042-M

CIE, 1955. Natural Daylight. Official Recommendation, Compte Rendu, CIE 13th Session, Committee E-3.2, vol. II, parts 3– 2, II–IV&35–37.

CIE, 1973. Standardization of luminance distribution on clear skies. Technical Report CIE 022:1973. CIE Technical Committee, Paris, France.

CIE, 1994. Guide to recommended practice of daylight measurement. Technical Report CIE 108:1994. CIE Central Bureau, Vienna, Austria.

CIE, 2014. CIE Standard General Sky Guide. Technical Report CIE 215:2014. CIE Central Bureau, Vienna, Austria.

Dumortier, D., Kobav, M.B., 2007. Deriving CIE sky types from horizontal irradiances, in: Proceedings of 26th Session of the CIE (Volume 1). Commission Internationale de L'Eclairage, Beijing.

Hoyer-Klick, C., Beyer, H.G., Dumortier, D., Schroedter-Homscheidt, M., Wald, L., Martinoli, M., Schilings, C., Gschwind, B., Menard, L., Gaboardi, E., Ramirez-Santigosa, L., Polo, J., Cebecauer, T., Huld, T., Suri, M., de Blas, M., Lorenz, E., Pfatischer, R., Remund, J., Ineichen, P., Tsvetkov, A., Hofierka, J., 2008. Management and exploitation of solar resource knowledge, in: Proceeding of the EUROSUN 2008, 1st International Conference on Solar Heating, Cooling and Buildings. Lisbon, Portugal.

Igawa, N., 2014. Improving the All Sky Model for the luminance and radiance distributions of the sky. Sol. Energy 105, 354–372. https://doi.org/10.1016/j.solener.2014.03.020

Igawa, N., Koga, Y., Matsuzawa, T., Nakamura, H., 2004. Models of sky radiance distribution and sky luminance distribution. Sol. Energy 77, 137–157. https://doi.org/10.1016/j.solener.2004.04.016

ISO 15469:2004(E)/CIE S 011/E:2003, 2004. Spatial Distribution of Daylight – CIE Standard General Sky. Geneva: ISO, Vienna: CIE.

Kittler, R., 1965. Standardisation of outdoor conditions for the calculation of daylight factor with clear skies, in: Proceedings of the CIE Intersessional Conference on Sunlight in Buildings. Newcastle upon Tyne, pp. 273–285.

Kittler, R., 1985. Luminance distribution characteristics of homogeneous skies: a measurement and prediction strategy. Light. Res. Technol. 17, 183–188. https://doi.org/10.1177/14771535850170040301

Kittler, R., 1993. Relative scattering indicatrix: Derivation from regular radiance/luminance distribution sky scans. Int. J. Light. Res. Technol. 25, 125–127. https://doi.org/10.1177/096032719302500302

Kittler, R., Darula, S., 2002. Parametric definition of the daylight climate. Renew. Energy 26, 177–187. https://doi.org/10.1016/S0960-1481(01)00128-8

Kittler, R., Hayman, S., Ruck, N., Julian, W., 1992. Daylight measurement data: Methods of evaluation and representation. Light. Res. Technol. 24, 173–187. https://doi.org/10.1177/096032719202400402

Kittler, R., Perez, R., Darula, S., 1997. A new generation of sky standards, in: Lux Europa. Proceedings of the Eight European Lighting Conference. Amsterdam, pp. 359–373.

Kittler, R., Perez, R., Darula, S., 1998. A set of standard skies characterizing daylight conditions for computer and energy conscious design. Am. - Slovak grant Proj. US - SK 92 052 92. https://doi.org/10.13140/RG.2.1.4798.7048

Kobav, M.B., Bizjak, G., Dumortier, D., 2012. Characterization of sky scanner measurements based on CIE and ISO standard CIE S 011/2003. Light. Res. Technol. 45, 504–512. https://doi.org/10.1177/1477153512458916

Kómar, L., Rusnák, A., Dubnička, R., 2013. Analysis of diffuse irradiance from two parts of sky vault divided by solar meridian using portable spectral sky-scanner. Sol. Energy 96, 1–9. https://doi.org/10.1016/J.SOLENER.2013.07.003

Li, D.H.W., Lam, T.N.T., Cheung, K.L., Tang, H.L., 2008. An analysis of luminous efficacies under the CIE standard skies. Renew. Energy. https://doi.org/10.1016/j.renene.2008.02.004

Li, D.H.W., Lau, C.C.S., Lam, J.C., 2003. A Study of 15 Sky Luminance Patterns against Hong Kong Data. Archit. Sci. Rev. 46, 61–68. https://doi.org/10.1080/00038628.2003.9696965

Li, D.H.W., Tang, H.L., 2008. Standard skies classification in Hong Kong. J. Atmos. Solar-Terrestrial Phys. 70, 1222–1230. https://doi.org/10.1016/J.JASTP.2008.03.004

Littlefair, P.J., 1994a. A comparison of sky luminance models with measured data from Garston, United Kingdom. Sol. Energy 53, 315–322. https://doi.org/10.1016/0038-092X(94)90034-5

Littlefair, P.J., 1994b. The luminance distributions of clear and quasi-clear skies, in: Proceedings of the CIBSE National Lighting Conference. Cambridge, UK, pp. 267–283.

Markou, M.T., Bartzokas, A., Kambezidis, H.D., 2007. A new statistical methodology for classification of sky luminance distributions based on scan data. Atmos. Res. 86, 261–277. https://doi.org/10.1016/j.atmosres.2007.06.001

Markou, M.T., Kambezidis, H.D., Bartzokas, A., Katsoulis, B.D., Muneer, T., 2005. Sky type classification in Central England during winter. Energy 30, 1667–1674. https://doi.org/10.1016/j.energy.2004.05.002

Matsuura, K., Iwata, T., 1990. A model of daylight source for the daylight illuminance calculations on the all weather conditions, in: Proceedings of 3rd International Daylighting Conference. Moscow, Russia.

Moon, P., Spencer, D.E., 1942. Illumination from a non-uniform sky. Trans. Illum. Eng. Soc. 37, 707–726.

Mukherjee, S., 2014. CIE standard general Sky type identification for Delhi during winter and summer. J. Opt. 43, 247–256. https://doi.org/10.1007/s12596-014-0218-5

Ng, E., Cheng, V., Gadi, Ankur, Mu, J., Lee, M., Gadi, Ankit, 2007. Defining standard skies for Hong Kong. Build. Environ. 42, 866–876. https://doi.org/10.1016/J.BUILDENV.2005.10.005

Perez, R., Ineichen, P., Seals, R., Michalsky, J.J., Stewart, R., 1990. Modeling daylight availability and irradiance components from direct and global irradiance. Sol. Energy 44, 271–289. https://doi.org/10.1016/0038-092X(90)90055-H

Perez, R., Seals, R., Michalsky, J.J., 1993. All-weather model for sky luminance distribution—Preliminary configuration and validation. Sol. Energy 50, 235–245. https://doi.org/10.1016/0038-092X(93)90017-I

Perraudeau, M., 1988. Luminance models, in: National Lighting Conference and Daylighting Colloquium. Cambridge, UK, pp. 291–292.

Suárez-García, A., Granados-López, D., González-Peña, D., Díez-Mediavilla, M., Alonso-Tristán, C., 2018. Seasonal caracterization of CIE standard sky types above Burgos, northwestern Spain. Sol. Energy 169, 24–33. https://doi.org/10.1016/J.SOLENER.2018.04.028

Torres, J.L., de Blas, M., García, A., Gracia, A.M., de Francisco, A., 2010a. Sky luminance distribution in Pamplona (Spain) during the summer period. J. Atmos. Solar-Terrestrial Phys. 72, 382–388. https://doi.org/10.1016/j.jastp.2009.12.005

Torres, J.L., de Blas, M., García, A., Gracia, A.M., de Francisco, A., 2010b. Sky luminance distribution in the North of Iberian Peninsula during winter. J. Atmos. Solar-Terrestrial Phys. 72, 1147–1154. https://doi.org/10.1016/j.jastp.2010.07.001

Torres, J.L., de Blas, M., Torres, L.M., García, A., de Francisco, A., 2014. Synthetic generation of standard sky types series using Markov Transition Matrices. Renew. Energy 62, 731–736. https://doi.org/10.1016/j.renene.2013.08.022

Tregenza, P.R., 1999. Standard skies for maritime climates. Light. Res. Technol. 31, 97–106. https://doi.org/10.1177/096032719903100304

Tregenza, P.R., 2004. Analysing sky luminance scans to obtain frequency distributions of CIE Standard General Skies. Light. Res. Technol. 36, 271–281. https://doi.org/10.1191/1477153504li117oa

Wittkopf, S.K., Soon, L.K.K., 2007. Analysing sky luminance scans and predicting frequent sky patterns in Singapore. Light. Res. Technol. 39, 31–51. https://doi.org/10.1177/1365782806070683